High-performance in n-type PbTe-based thermoelectric materials achieved by synergistically dynamic doping and energy filtering

Hang-Tian Liu,[a,#] *Qiang Sun,*[b,c,#] *Yan Zhong,*[a] *Qian Deng,*[a] *Lin Gan,*[a] *Fang-Lin Lv,*[a] *Xiao-Lei Shi,*[d,b,e] *Zhi-Gang Chen,*[d,e,*] *and Ran Ang* [a,f,*]

a Key Laboratory of Radiation Physics and Technology, Ministry of Education, Institute of Nuclear Science and Technology, Sichuan University, Chengdu 610064, China

b School of Mechanical and Mining Engineering, University of Queensland, Brisbane, Queensland 4072, Australia

c Centre for Microscopy and Microanalysis, University of Queensland, Brisbane, Queensland 4072, Australia

d Centre for Future Materials, University of Southern Queensland, Springfield central, Queensland 4300, Australia

e School of Chemistry and Physics, Queensland University of Technology, Brisbane City, Queensland 4000, Australia

f Institute of New Energy and Low-Carbon Technology, Sichuan University, Chengdu 610065, China

*Corresponding authors and Emails: rang@scu.edu.cn (RA), zhigang.chen@usq.edu.au (ZGC)

[#] Hang-Tian Liu and Qiang Sun contributes equally to this work.

Abstract

The development of n-type high-performance PbTe thermoelectric materials for matching its p-type counterparts is an urgent matter to expand its practical applications. Here, we introduce Ag_2Te into n-type $Pb_{0.975}Cr_{0.025}Te$ for achieving a high peak figure of merit of 1.5 at 773 K. Such a high value is attributed to the synergistic optimization of carrier and phonon transports by Ag_2Te introducing and the dynamic doping of Ag. From the detailed structure and property analysis, we found that Ag_2Te nanoprecipitates establish coherent interfaces and hence potential barriers with the matrix to induce energy-dependent carrier scattering and maintain relatively high carrier mobility, leading to an optimal electrical-transport properties over a wide temperature range. Moreover, we employ comprehensive electron microscopy investigations and approximate Debye-Callaway model to reveal the origin of the significantly reduced lattice thermal conductivity in Ag_2Te-alloyed $Pb_{0.975}Cr_{0.025}Te$. The strategies used here provide an effective method for designing high-performance thermoelectric material systems.
Keywords: thermoelectric; n-type PbTe; Ag_2Te; dynamic doping; coherent interfaces; energy filtering

1. Introduction

Thermoelectric technology, enabling the direct conversion between heat and electricity based on the Seebeck and Peltier effects, is expected to solve the issues of energy shortage and environmental pollution [1-4]. To evaluate the conversion efficiency of a thermoelectric material, either as a refrigerator or a generator, the dimensionless thermoelectric figure of merit ZT is defined as $ZT = S^2\sigma T/\kappa$, where S, σ, κ and T are the Seebeck coefficient, electrical conductivity, thermal conductivity, and the absolute temperature. Generally, thermoelectric power factor ($S^2\sigma$) reflects the electrical-transport properties and the thermal conductivity κ determines the thermal-transport properties and is composed of the electronic thermal conductivity (κ_E) and the lattice thermal conductivity (κ_L) [5]. Thus, an ideal thermoelectric material requires high $S^2\sigma$ and low κ simultaneously, achieved by band structure engineering, optimizing carrier concentration (n), lattice anharmonicity, nanostructuring, and porosity design [6-9].

The inherent low κ_L, caused by high bonding anharmonicity and soft phonon behavior, makes PbTe an ideal mid-temperature thermoelectric material [10]. However, unlike that in p-type PbTe where both the light (L point) and heavy (Σ point) hole bands participate in hole transport, only one conduction band in n-type PbTe participates in the electron transport, which hinders the large-scale commercial application of PbTe [11,12]. To solve this matter, numerous efforts are aimed at improving the $S^2\sigma$ of n-type PbTe to match their p-type counterparts, mainly including two primary approaches: (1) heterovalent element doping or dynamic doping to optimize n for increasing σ [13-18]; (2) band structure engineering to increase S (including conduction band flattening [19], resonant levels [20,21] or energy filtering effect [22]). However, the mutual coupling of thermoelectric parameters complicates the simultaneous optimization of σ and S [23]. Therefore, screening a single compound dopant, which can simultaneously introduce dynamic doping and energy filtering effects into PbTe, is expected to be an effective approach for enhancing the electrical transport properties.

Ag exhibits a temperature-dependent solubility in PbTe, indicating the potential of dynamically optimizing *n* [24]. Recently, both PbTe-Ag_2Te heterostructures and Ag-rich nanodots embedded PbTe has been reported to block the detrimental minority carriers, leading to enhanced *ZT* [25,26]. However, the mismatched interface between the nanoprecipitate and the matrix can cause severe carrier scattering, leading to reduced carrier mobility μ and electrical transport properties [27,28]. To solve this challenge, we synthesized a series of $Pb_{0.975}Cr_{0.025}Te$-*x*Ag_2Te compounds *via* a vacuum melting followed by hot pressing and investigated the behavior of Ag in Ag_2Te-alloyed $Pb_{0.975}Cr_{0.025}Te$. Interestingly, our comprehensive experimental results indicate that excessive doping of Ag in $Pb_{0.975}Cr_{0.025}Te$ introduces dynamic doping and establishes coherent interface potential barriers between the Ag_2Te nanoprecipitate and the matrix, which realizes energy-dependent carrier scattering and band alignment with relatively high μ, leading to increased $S^2\sigma$. On the other hand, the introduction of point defects, nanostructures, and mesoscale structures, induced by Ag_2Te alloying, plays a predominant role in significantly suppressed κ_L [9,28]. Furthermore, our developed Debye-Callaway model illustrates the underlying mechanism to the reduction of κ_L. Benefiting from the synergistically optimized carrier and phonon transports by the incorporation of Cr and Ag, a peak *ZT* of ~1.5 at 773 K and an average ZT_{ave} of ~0.93 from 323 to 823 K with a calculated conversion efficiency of ~ 13.2% are achieved in $Pb_{0.975}Cr_{0.025}Te$-1.5% Ag_2Te.

2. Experimental section

2.1 Material synthesis.

Stoichiometric high-purity elements [Pb (99.99%), Te (99.999%), Cr (99.999%), and Ag (99.999%)] were sealed in vacuum quartz tubes, heated to 1373 K within 6 h, and held for 6h. After quenched in ice water, quartz tubes were annealed at 873 K for 72h to synthesize polycrystalline n-type $Pb_{0.975}Cr_{0.025}Te$-*x*Ag_2Te (*x*=0, 0.5%, 1.0%, 1.5%, 2.0%). The obtained ingots were crushed into fine powders, then sintered into disk-shaped specimens with a diameter of 12.5 mm *via* rapid hot pressing at 873 K for 45 minutes with a 50 MPa uniaxial pressure. The densities of obtained disks were

measured by the Archimedes method and confirmed to be higher than 97% of the theoretical density (**Table S1**).

2.2 Phase and microstructure characterization.

Powder X-ray diffraction (XRD) measurements were performed on an X-ray diffractometer using Cu–Kα radiation. The morphological, structural, and chemical characteristics of the synthesized samples were investigated by the scanning electron microscopy (SEM, JEOL 7100, equipped with electron backscatter diffraction detector) and probe-corrected STEM/TEM (Hitachi HF5000, equipped with energy-dispersive X-ray spectroscopy (EDS) detector and secondary electron detector). The cross-sectional TEM specimens were prepared by the FEI Scios focus ion beam system.

2.3 Thermoelectric property measurement.

The S and σ were performed using a CTApro (Beijing Cryoall Science and Technology Co., Ltd, China) instrument in a helium atmosphere from 300 K to 873 K. The thermal diffusivity D was performed by the laser flash method (NETZSCH, LFA 467) from 300 K to 873 K. The heat capacity C_p was determined from the measurements of Blachnik by $C_p(k_B/atom) = 3.07 + 0.00047(T/K-300)$ for PbTe [29]. The Hall carrier concentration n_H and Hall mobility μ_H were determined by Hall measurements using a Van der Pauw technique.

3. Result and discussion

Ag_2Te was found to strongly change structures and electrical properties of $Pb_{0.975}Cr_{0.025}Te$. **Fig. S1**a displays room temperature X-ray diffraction (XRD) patterns for the $Pb_{0.975}Cr_{0.025}Te$-$x$$Ag_2Te$ (x=0, 0.5%, 1.0%, 1.5%, 2.0%). It can be seen that the samples are crystallized in the cubic rock-salt PbTe structure (space group *Fm-3m*) and no obvious impurities are observed within the detection limit. The lattice parameter (a) increases slightly with increasing the Ag_2Te content due to the larger ionic radius of Ag^+ (~1.26 Å) than Pb^{2+} (~1.2 Å) and Cr^{2+} (~0.84 Å), as shown in **Fig. S1**b. **Fig. 1** shows temperature-dependent σ, S, n_H, and μ_H of the $Pb_{0.975}Cr_{0.025}Te$-$x$$Ag_2Te$ (x=0, 0.5%, 1.0%, 1.5%, 2.0%). As can be seen, the increased σ and decreased /S/ with increasing the temperature is opposite to the

behavior of $Pb_{0.975}Cr_{0.025}Te$, showing a typical temperature-dependent n_H caused by the temperature-induced increase of Ag solubility in PbTe [24], as shown in **Fig. 1**c. At the near-room temperature, the simultaneous decrease of n_H and μ_H causes σ to decrease from ~847 S cm^{-1} of $Pb_{0.975}Cr_{0.025}Te$ to ~201 S cm^{-1} of $Pb_{0.975}Cr_{0.025}Te$-0.5%Ag_2Te. Generally, as the composition increases, a decrease in n_H at room temperature will increase μ_H, and the decreasing μ_H indicates the presence of additional carrier scattering sources [30]. This observation can be further confirmed by the temperature-dependent μ_H for all $Pb_{0.975}Cr_{0.025}Te$-$x$$Ag_2Te$ samples in **Fig. 1**d, which gradually deviates from the tendency of $T^{-2.75}$ (a typical case of the dominant charge carrier scattering by acoustic phonons in n-type PbTe) upon the increased Ag_2Te content [24]. The room-temperature S increases from ~199 μV K^{-1} of the $Pb_{0.975}Cr_{0.025}Te$ to ~296 μV K^{-1} of the $Pb_{0.975}Cr_{0.025}Te$-0.5%Ag_2Te, while the room-temperature n_H only decreases from ~3.63×10^{18} cm^{-3} of the $Pb_{0.975}Cr_{0.025}Te$ to ~2.72×10^{18} cm^{-3} of the $Pb_{0.975}Cr_{0.025}Te$-0.5%Ag_2Te, indicating an uncertain factor must rise in the band structure or trigger energy filtering effect.

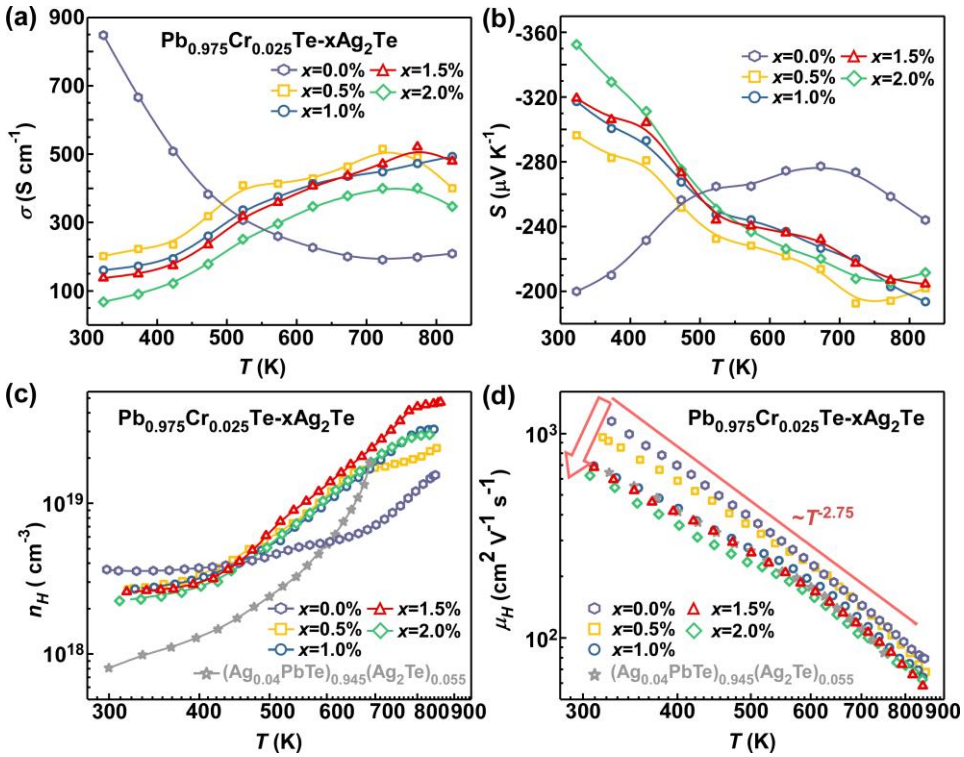

Fig. 1. Temperature-dependent (a) electrical conductivity σ, (b) Seebeck coefficient S, (c) Hall carrier concentration n_H, and (d) Hall carrier mobility for the $Pb_{0.975}Cr_{0.025}Te$-xAg_2Te (x=0, 0.5%, 1.0%, 1.5%, 2.0%).

To reveal the origin of the abnormally increased S, the single Kane band (SKB) model was used to identify changes in the band structure [31]. As shown in **Fig. 2**a, the S of the PbAgTe:Ag_2Te is well consistent with the Pisarenko line assuming the effective mass m^* of 0.25m_e, indicating that the band structure is not significantly altered by Ag at the different content in this work [24]. In our previous work, Cr-doped PbTe with m^* of 0.30 m_e was confirmed to possess resonant levels effect [32]. For the Ag_2Te-alloyed $Pb_{0.975}Cr_{0.025}Te$, the S is overall higher than those at the curve of 0.30m_e and gradually deviates from the curve with increasing the Ag_2Te content, indicating that the abnormally decreased μ_H and increased S come from the energy filtering effect rather than the changed band structure. It should be mentioned that the energy filtering effect can be manifested by the bending of the charge carrier band formed at the nanoprecipitate-matrix interface, which acts as a slowly changing potential

with sufficient strength to scatter low-energy carriers [22,33]. Generally, these nanoprecipitate scattering sources as the second phase impurities cannot change the band structure of the matrix, leading to the modulated scattering parameter r_x without affecting m^* [34]. Since acoustic phonon scattering is the dominant carrier-scattering mechanism, the scattering parameter of $Pb_{0.975}Cr_{0.025}Te$ (r_0) should be -0.5 at room temperature. The ratio of the scattering parameter r_x+1 for $Pb_{0.975}Cr_{0.025}Te$-$x$$Ag_2Te$ (x=0.5%, 1.0%, 1.5%, 2.0%) to r_0+1 can be expressed as [34]:

$$\frac{r_x+1}{r_0+1}=\frac{S_x}{S_0}\left(\frac{n_x}{n_0}\right)^{2/3} \tag{1}$$

which is modified from [35]:

$$S=\left[8\pi^2k_B^2/\left(3eh^2\right)\right]m^*T\left[\pi/\left(3n\right)\right]^{2/3}\left(r+1\right) \tag{2}$$

where S_x (S_0) and n_x (n_0) are the measured S and n at room temperature, k_B is the Boltzmann constant, and h is the Planck constant. As shown in **Fig. 2**b, the calculated r_x increases significantly with increasing the Ag_2Te content, confirming that the enhancement in S is attributable to the enlarged r_x by adding nanoprecipitates.

To comprehensively elucidate the effects of energy-dependent carrier scattering, we calculated the interface potential barriers (E_b) between the nanoprecipitates and the matrix, which is assumed to be related to σ, expressed as [36]:

$$\sigma \propto T^{1/2}\exp\left(-\frac{E_b}{k_BT}\right) \tag{3}$$

Fig. 2c displays a plot of $\ln(\sigma T^{1/2})$ versus $1/(k_BT)$ for the $Pb_{0.975}Cr_{0.025}Te$-$x$$Ag_2Te$, and a good linear relationship can be observed, indicating the rationality of this assumption. As shown in **Fig. 2**b, the obtained absolute values of interface potential barriers $|E_b|$ increase with increasing the Ag_2Te content, indicating that the number of interfaces or phase boundaries was increased by the introduction of Ag_2Te. However, forming interfaces or phase boundaries causes the deterioration of μ and in turn the electrical transport properties [37]. As shown in **Fig. 2**d, the room-temperature μ_H decreases after

introducing Ag_2Te, but it is still superior to other reported Ag-doped PbTe systems [26,38] and is close to PbAgTe: Ag_2Te samples with lower n_H [24], revealing the special coherence between the nanoparticles and the matrix in the Ag_2Te-alloyed $Pb_{0.975}Cr_{0.025}Te$.

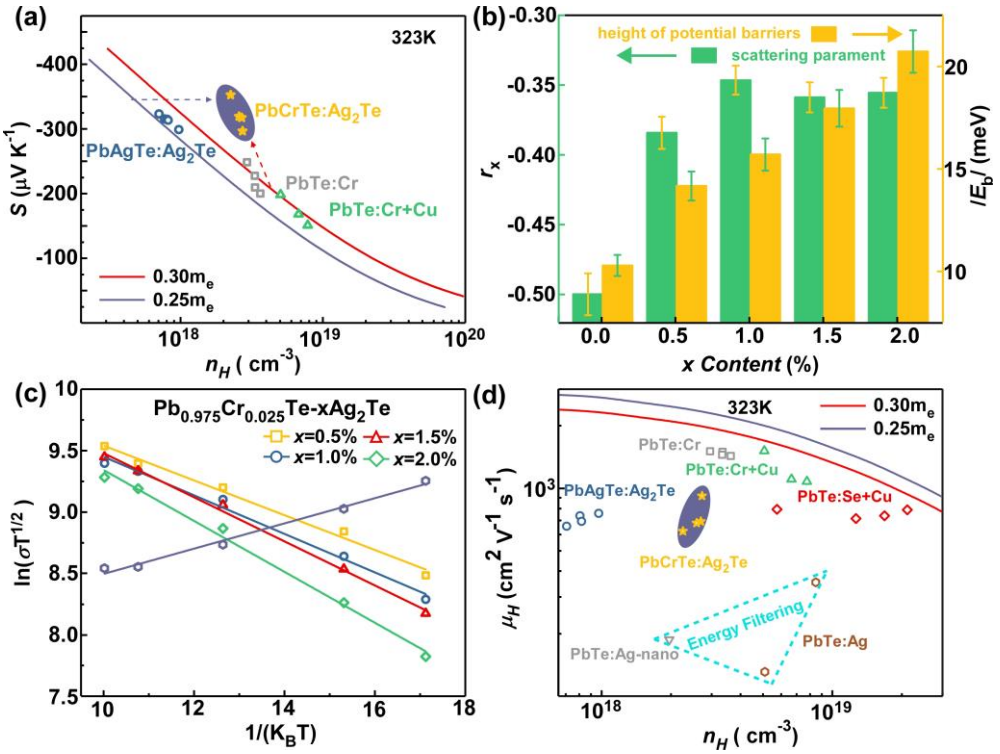

Fig. 2. (a) Room-temperature S as a function of n_H, with a comparison to theoretical predictions and literature results [24,32]. (b) Calculated scattering parameter r_x and interface potential barriers E_b as a function of Ag_2Te content. (c)The plot of $\ln(\sigma T^{1/2})$ versus $1/(k_BT)$. (d) Room-temperature μ_H as a function of n_H, with a comparison to theoretical line and literature results [14,24,26,32,38].

To verify the roles of Ag_2Te in achieving the observed electronic transport properties, we carried out comprehensive electron microscopy investigations to examine the nanostructure at the $Pb_{0.975}Cr_{0.025}Te$-1.5%Ag_2Te. **Fig. 3**a is a high-angle annular dark-field (HAADF) STEM image of the $Pb_{0.975}Cr_{0.025}Te$-1.5%Ag_2Te, displaying that the micron-sized second phase and high density of nanoprecipitates are embedded in the matrix. To confirm the chemical characteristics of the $Pb_{0.975}Cr_{0.025}Te$-1.5%Ag_2Te, the energy dispersive spectrometry (EDS) elemental maps of Pb, Te, Ag,

and Cr are shown in **Fig. 3**b-c, indicating that the secondary phase is Cr-enriched while the nanoprecipitates are Ag-enriched. **Fig. 3**d shows a bright-field transmission electron microscopy (BF-TEM) image, with a high density of Ag-enriched nanosized precipitates marked. **Fig. 3**e shows a high-resolution TEM (HRTEM) image of the interface between the PbTe matrix and the nanoprecipitate, which is sharp and coherent. Based on the crystallographic analysis, the nanoprecipitates adopt the β-Ag_2Te phase (Space Group *P121*). To understand the orientation relationship at the interface, the selected area electron diffraction (SAED) pattern was obtained from the interface, as shown in **Fig. 3**f. After carefully indexing the overlapped diffraction pattern, the orientation relationships of $(1\bar{1}\bar{1})_{PbTe}$// $(10\bar{1})_{Ag2Te}$ and $(1\bar{1}3)_{PbTe}$//$(0\bar{1}1)_{Ag2Te}$ can be confirmed. Based on the crystallographic analysis, 2d $(1\bar{1}\bar{1})_{PbTe}$=7.46 Å, d $(10\bar{1})_{Ag2Te}$=7.52 Å; 2d$(1\bar{1}3)_{PbTe}$=3.90 Å, d$(0\bar{1}1)_{Ag2Te}$=3.83 Å. Therefore, the lattice mismatches between these parallel planes are less than 2%, leading to the formation of the coherent interface. **Fig. 3**g shows an enlarged HRTEM image displaying the orientation relationship, which can be conducive to maintaining relatively high μ. **Fig. 3**h shows the schematic atomic model. To understand the energy filtering effect triggered by Ag_2Te nanoprecipitates embed in the matrix, the assumed band alignment between Ag_2Te and PbTe is schematically illustrated in **Fig. 3**i. As can be seen, due to the large bandgap difference (~0.05eV for Ag_2Te and ~0.30eV for PbTe at room temperature) [39,40], the discontinuity of the conduction band and the valence band is form electron and hole barriers for scattering low energy carriers and thus gives rise to increased *S* [41].

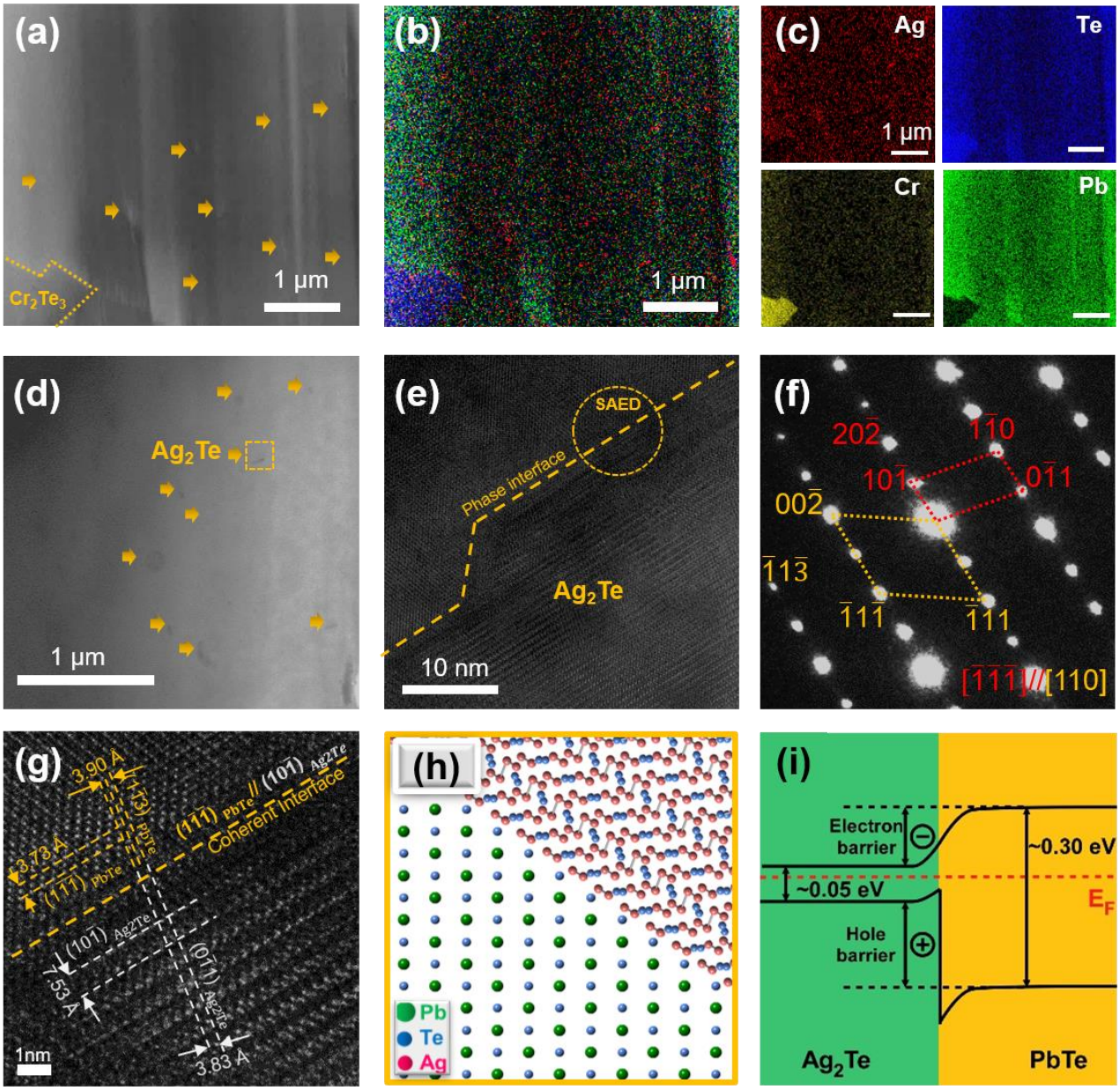

Fig. 3. Structural and compositional characterizations of the $Pb_{0.975}Cr_{0.025}Te$-1.5%Ag_2Te. (a) HAADF-STEM image of $Pb_{0.975}Cr_{0.025}Te$-1.5%Ag_2Te, containing micron-sized second phase and a high density of nanoprecipitates. (b) and (c) elemental maps for the elemental distributions of Pb, Te, Cr, and Ag. (d) BF-TEM image of the dense Ag-enriched nano-precipitates. (e) HRTEM image of an interface between PbTe and Ag_2Te. (f) The SAED image obtained from the marked region in (e). (g) Enlarged HRTEM image showing the detailed orientation relationship analysis and (h) corresponding atomic model. (i) The schematic band alignment between Ag_2Te and PbTe.

Since the microstructure/nanostructure of the $Pb_{0.975}Cr_{0.025}Te$-xAg_2Te can influence the phonon scattering and reduce κ, we further systematically examined the microstructures of the $Pb_{0.975}Cr_{0.025}Te$-1.5%Ag_2Te. **Fig. 4**a shows a BF-TEM image of the phase boundary between the Cr_2Te_3 and matrix, in which the rock-salt structured PbTe is aligned along its [112] zone-axis. **Fig. 4**b shows the EDS quantitative analysis, suggesting that the atomic ratio of Cr:Te = 2:3, and the matrix composition is Ag-doped PbTe with a small amount of Cr, explaining the decreased n_H at the room temperature. **Fig. 4**c shows an HRTEM image along the [112] direction, obtained from a typical area from the matrix. Its atomic-resolution HAADF STEM image is shown in **Fig. 4**d. As can be seen, the Z-contrast derived from different atoms, and dense lattice distortion can be induced massive point defects. **Fig. 4**e shows an HRTEM image containing grain boundaries and phase interfaces, in which intense strain fields can be seen in the area close to interfaces. **Fig. 4**f shows a corresponding enlarged HRTEM image, in which the *d* spacing of [002] planes of Cr_2Te_3 can be observed. The existence of point defects, nanostructures, and mesoscale structures introduced by Cr and Ag doping in PbTe play significant roles in scattering phonons from low to high wavelengths and in turn results in an ultra-low κ_L.

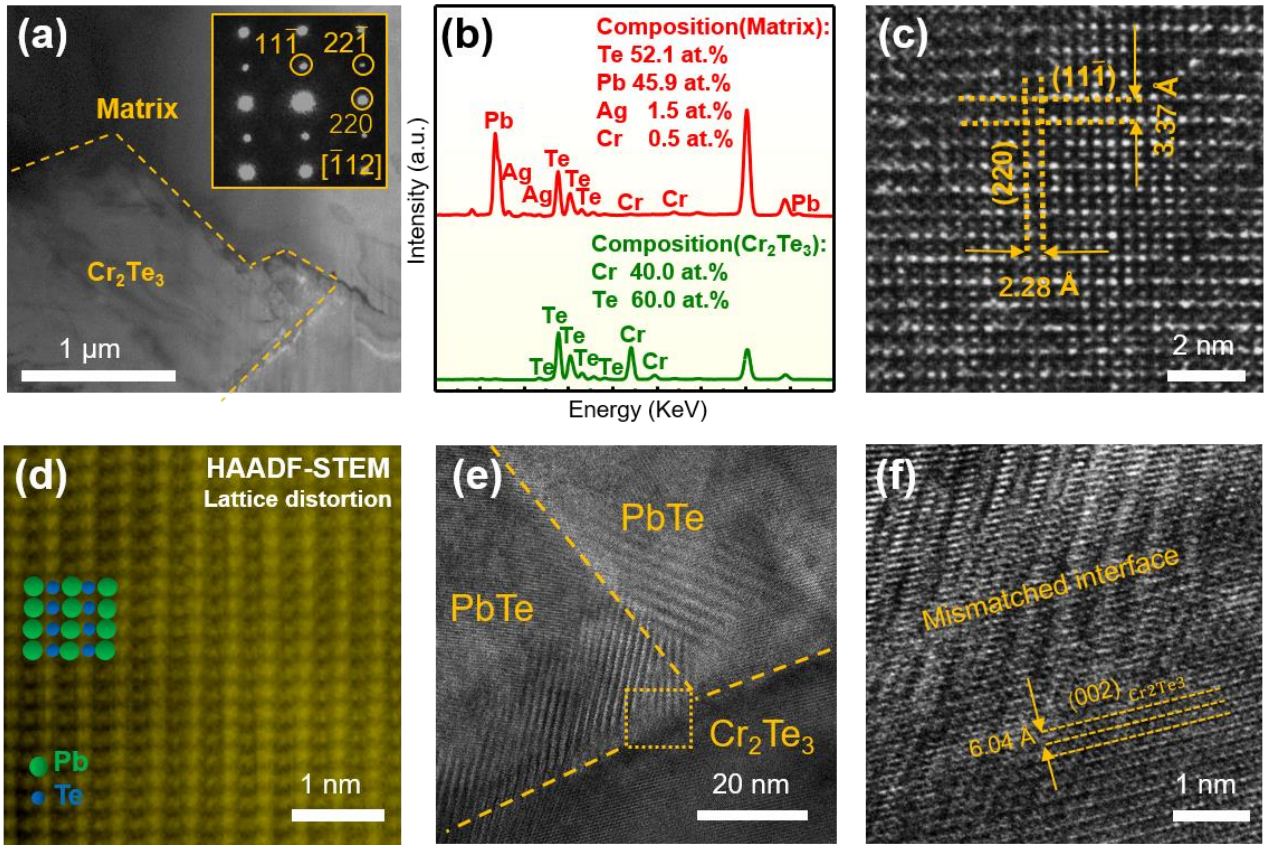

Fig. 4. Structural and compositional characterization of the $Pb_{0.975}Cr_{0.025}Te$-1.5%Ag_2Te. (a) BF-TEM image showing the microstructure, inset displaying the [112] zone-axis diffraction pattern of PbTe. (b) EDS spectra obtained from the PbTe matrix and Cr_2Te_3 secondary phase. (c) HRTEM image of PbTe viewing along the [112] zone-axis. (d) Atomic-resolution HAADF STEM image of PbTe, showing dense lattice distortion. (e) HRTEM image of mismatched grain boundary between Cr_2Te_3 and PbTe, with corresponding enlarged HRTEM images shown in (f).

As shown in **Fig. 5**a, the $S^2\sigma$ of the $Pb_{0.975}Cr_{0.025}Te$-$x$$Ag_2Te$ increases with increasing the temperature, reaching a peak value of 23.5 μW cm^{-1} K^{-2} at 673 K in $Pb_{0.975}Cr_{0.025}Te$-1.5%Ag_2Te. **Fig. 5**b shows the total thermal conductivity (κ) and lattice thermal conductivity (κ_L) as a function of temperature. The $\kappa=DC_p\rho=\kappa_L+L\sigma T$, where D, C_p, ρ, and L are thermal diffusivity, heat capacity, density, and Lorenz number [42,43]. All the measured and calculated results are shown in **Fig. S2** and **Table S1**. The minimum κ_L notably decreases from 0.90 $Wm^{-1}K^{-1}$ of the $Pb_{0.975}Cr_{0.025}Te$ to 0.49 Wm^{-}

$^{1}K^{-1}$ of the $Pb_{0.975}Cr_{0.025}Te$-1.5%Ag_2Te. Ag_2Te nanoprecipitates can effectively intensify the phonon scattering and maintain relatively high μ due to the coherent interface. We further compared the ratio of μ_H/κ_L as well as the minimum κ_L in **Fig. 5**c. Compared with the previously reported n-type PbTe containing Ag or energy filtering [24,44-47], the $Pb_{0.975}Cr_{0.025}Te$-1.5%Ag_2Te shows an excellent μ_H/κ_L and relatively low minimum κ_L, indicating Ag_2Te nanoprecipitates can simultaneously optimize carrier and phonon transport in this work. To investigate the individual contribution of six dominant phonon scattering sources, including Umklapp process (U), normal process (N), grain boundary (GB) scattering, point defect (PD) scattering, micro precipitate (MP) scattering, and nano precipitate (NP) scattering, we employed the Debye-Callaway model in Ag_2Te-alloyed $Pb_{0.975}Cr_{0.025}Te$. The spectral lattice thermal conductivity (κ_s) can be calculated by [48,49]:

$$\kappa_s = \frac{k_B}{2\pi^2 v}\left(\frac{k_B T}{\hbar}\right)^3 \tau_{tot} \frac{x^4 e^x}{\left(e^x - 1\right)^2} \tag{4}$$

where v is the sound velocity (plot in **Fig. S3**), $\hbar$ is Plank's reduced constant, x is defined as $x = \hbar\omega/k_B T$ (with ω denoting the phonon frequency), and τ_{tot} is combined relaxation time. More calculation details are presented in the Supporting Information. **Fig. 5**d shows the calculated κ_s with respect to ω by models of U+N, U+N+GB, U+N+GB+PD, U+N+GB+PD+MP, U+N+GB+PD+MP+NP at 300 K. The colored area between the curves is the degree of κ_L reduction caused by the introduction of an additional phonon scattering center. It can be seen that GB and MP only perform a small magnitude of scattering phonon in the low-frequency range because of the relatively large grain size. Notably, the introduction of high-density Ag_2Te nanoprecipitates and point defects remarkably reduce κ_L contributed by low-frequency and high-frequency phonons, respectively. Therefore, optimizing phonon scattering sources by Ag_2Te doping can significantly reduce κ_L of the Cr-alloyed PbTe, securing high thermoelectric performance. To sum up, the introduction of Ag_2Te nanoprecipitates not only optimizes n in a wide temperature range, but also builds interface potential barriers to scatter low-energy carriers, leading to the improvement of electrical transport properties.

Consequently, an outstanding peak ZT ~1.5 at 773K is achieved in the $Pb_{0.975}Cr_{0.025}Te$-1.5%Ag_2Te, as shown in **Fig. 5**e. A high average ZT_{ave} ~0.93 with the corresponding calculated conversion efficiency η ~ 13.3% can be obtained in the entire measured temperature (**Fig. S4**). To our best knowledge, such an excellent overall ZT is competitive to most cutting-of-edge n-type PbTe systems containing Ag or energy filtering (**Fig. 5**f) [24,46-49]. Additionally, the repeated measurement results of the $Pb_{0.975}Cr_{0.025}Te$-1.5%Ag_2Te (**Fig. S5**) indicate that our sample possesses good thermal stability and reproducibility, showing great potentials in the practical device application.

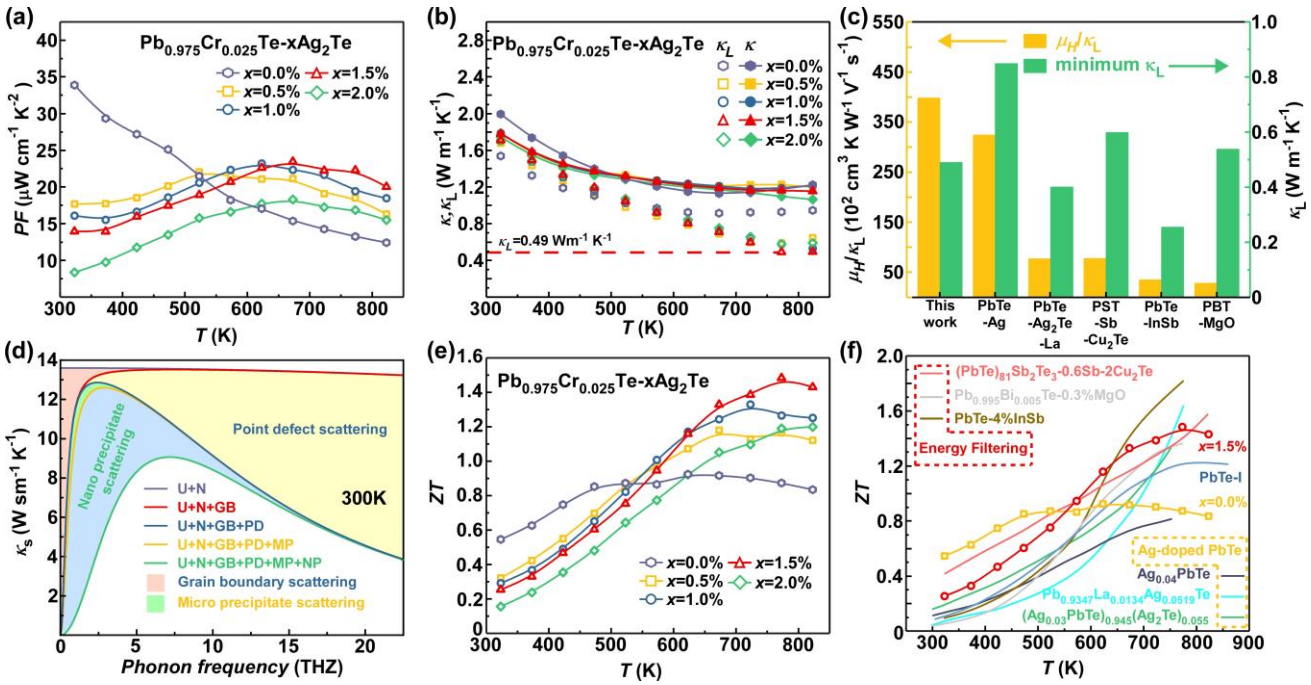

Fig. 5. (a) Temperature-dependent $S^2\sigma$ (PF). (b) Temperature-dependent the total thermal conductivity (κ) and the lattice thermal conductivity (κ_L). (c) μ_H/κ_L and the minimum κ_L of the $Pb_{0.975}Cr_{0.025}Te$-1.5%Ag_2Te with previous samples containing Ag or energy filtering. PbTe-Ag [24], PbTe-Ag_2Te-La [44], PST-Sb-Cu_2Te [45], PbTe-InSb [46], PBT-MgO [47]. (d) Calculated spectral lattice thermal conductivity κ_s of Ag_2Te-doped $Pb_{0.975}Cr_{0.025}Te$ sample based on the Debye-Callaway model at 300K. (e) Temperature-dependent ZT and (f) compare with previous samples containing Ag or energy filtering [24,44-47,50].

4. Conclusion

For the first time, we demonstrate the synergy of dynamic doping and energy filtering by introducing Ag_2Te nanoprecipitates to realize optimized electrical transport performance in the Cr-doped PbTe. The temperature-induced gradual increase in Ag solubility causes a dynamical carrier concentration and the nanoprecipitate-matrix coherent interface can establish potential barriers for energy-selective carrier scattering, thereby increasing the Seebeck coefficient, maintaining relatively high mobility, and in turn enhancing power factor. Simultaneously, the detailed microstructure of Ag and Cr co-doped PbTe was uncovered by our comprehensive electron microscopy studies, displaying dense lattice distortion, coherent Ag_2Te nanoprecipitates, and microscale Cr_2Te_3 secondary phase, which can scatter phonons to varying degrees and jointly suppress thermal transports. Consequently, the combination of both optimized carrier and phonon transport leads to a peak ZT of 1.5 at 773K in $Pb_{0.975}Cr_{0.025}Te$-1.5%Ag_2Te and the average ZT_{ave} ~0.93 from 323 K to 823K temperature range. The strategies in this work can provide a new venue for maximizing the performance of thermoelectric materials.

Acknowledgements

Hangtian Liu and Qiang Sun contributes equally to this work. This work was financially supported by the National Key Research and Development Program of China (Grant No. 2018YFA0702100), the National Natural Science Foundation (NNSF) of China (Grant No. 51771126), the Joint Funds of the NNSF of China and the Chinese Academy of Sciences' Large-Scale Scientific Facility (Grant No. U1932106), Sichuan University Innovation Research Program of China (Grant No. 2020SCUNL112). ZGC thanks the financial support from the Australian Research Council and HBIS-UQ Innovation Centre for Sustainable Steel (ICSS) project. The authors acknowledge the facilities, and the scientific and technical assistance, of the Australian Microscopy & Microanalysis Research Facility at the Centre for Microscopy and Microanalysis, The University of Queensland. The authors thank Prof. Yanzhong Pei from Tongji University for his support and discussion on Hall measurement.

Appendix A. Supporting information

Modelling study details. Density, XRD patterns and calculated lattice parameter *a*, thermal diffusivity, heat capacity, Lorenz number, electronic thermal conductivity, sound velocities, ZT_{ave} and corresponding calculated conversion efficiency η of $Pb_{0.975}Cr_{0.025}Te$-xAg_2Te. Repeated property measurement results of $Pb_{0.975}Cr_{0.025}Te$-1.5% Ag_2Te.

REFERENCES

[1] J. He, T.M. Tritt, Advances in thermoelectric materials research: Looking back and moving forward, Science 357 (2017) 1369.

[2] Q.H. Zhang, X.Y. Huang, S.Q. Bai, X. Shi, C. Uher, L.-D. Chen, Thermoelectric devices for power generation: recent progress and future challenges, Adv. Eng. Mater. 18 (2016) 194-213.

[3] X.L. Shi, J. Zou, Z.-G. Chen, Advanced thermoelectric design: from materials and structures to devices, Chem. Rev. 120 (2020) 7399-7515.

[4] M. Haras, T. Skotnicki, Thermoelectricity for IoT – a review, Nano Energy. 54 (2018) 461-476.

[5] G.J. Snyder, E.S. Toberer, Complex thermoelectric materials, Nat. Mater. 7 (2008) 105-114.

[6] Y.Z. Pei, H. Wang, G.J. Snyder, Band engineering of thermoelectric materials, Adv. Mater. 24 (2012) 6125-6135.

[7] L.D. Zhao, V.P. Dravid, M.G. Kanatzidis, The panoscopic approach to high performance thermoelectrics. Energy Environ. Sci. 7 (2014) 251-268.

[8] H. Wu, X. Lu, G. Wang, K. Peng, B. Zhang, Y. Chen, X. Gong, X. Tang, X. Zhang, Z. Feng, G. Han, Y. Zhang, X. Zhou, Strong lattice anharmonicity securing intrinsically low lattice thermal conductivity and high performance thermoelectric $SnSb_2Te_4$ via Se alloying, Nano Energy. 76 (2020) 105084.

[9] G.J. Tan, L.D. Zhao, M.G. Kanatzidis, Rationally designing high-performance bulk thermoelectric materials, Chem. Rev. 116 (2016) 12123-12149.

[10] E.S. Božin, C.D. Malliakas, P. Souvatzis, T. Proffen, N.A. Spaldin, M.G. Kanatzidis, S.J.L. Billinge, Entropically stabilized local dipole formation in lead chalcogenides, Science 330 (2010) 1660-1663.

[11] H. Sitter, K. Lischka, H. Heinrich, Structure of the second valence band in PbTe, Phys. Rev. B 16 (1977) 680-687.

[12] Y. Takagiwa, Y.Z. Pei, G. Pomrehn, G.J. Snyder, Validity of rigid band approximation of PbTe

thermoelectric materials, APL Mater. 1 (2013) 011101.

[13] Q. Zhang, E.K. Chere, Y.M. Wang, H. Kim, R. He, F. Cao, K. Dahal, D. Broido, G. Chen, Z.F. Ren, High thermoelectric performance of n-type $PbTe_{1-y}S_y$ due to deep lying states induced by indium doping and spinodal decomposition, Nano Energy. 22 (2016) 572-582.

[14] Y.W. Xiao, Y.X. Wu, P.F. Nan, H.L. Dong, Z.W. Chen, Z.Q. Chen, H.K. Gu, B.H. Ge, W. Li, Y.Z. Pei, Cu Interstitials Enable Carriers and Dislocations for Thermoelectric Enhancements in n-$PbTe_{0.75}Se_{0.25}$, Chem. 6 (2020) 523-537.

[15] Y. Xiao, H.J. Wu, W. Li, M.J. Yin, Y.L. Pei, Y. Zhang, L.W. Fu, Y.X. Chen, S.J. Pennycook, L. Huang, J.Q. He, L.D. Zhao, Remarkable roles of Cu to synergistically optimize phonon and carrier transport in n-type PbTe-Cu_2Te, J. Am. Chem. Soc. 139 (2017) 18732-18738.

[16] G.J. Tan, C.C. Stoumpos, S. Wang, T.P. Bailey, L.D. Zhao, C. Uher, M.G. Kanatzidis, Subtle roles of Sb and S in regulating the thermoelectric properties of n-type PbTe to high performance, Adv. Energy Mater. 7 (2017) 1700099.

[17] Q. Zhang, Q.C Song, X.Y. Wang, J.Y Sun, Q. Zhu, K. Dahal, X. Lin, F. Cao, J.W. Zhou, S. Chen, G. Chen, J. Mao, Z.F. Ren, Deep defect level engineering: a strategy of optimizing the carrier concentration for high thermoelectric performance, Energy Environ. Sci. 11 (2018) 933-940.

[18] X.L. Su, S.Q. Hao, T.P. Bailey, S. Wang, I. Hadar, G.J. Tan, T.B. Song, Q.J. Zhang, C. Uher, C. Wolverton, X.F. Tang, M.G. Kanatzidis, Weak Electron Phonon Coupling and Deep Level Impurity for High Thermoelectric Performance $Pb_{1-x}Ga_xTe$, Adv. Energy Mater. 8 (2018) 1800659.

[19] Y. Xiao, H.J. Wu, J. Cui, D.Y. Wang, L.W. Fu, Y. Zhang, Y. Chen, J.Q. He, S.J. Pennycook, L.D. Zhao, Realizing high performance n-type PbTe by synergistically optimizing effective mass and carrier mobility and suppressing bipolar thermal conductivity, Energy Environ. Sci. 11 (2018) 2486-2495.

[20] J.P. Heremans, B. Wiendlocha, A.M. Chamoire, Resonant levels in bulk thermoelectric semiconductors, Energy Environ. Sci. 5 (2012) 5510-5530.

[21] K. Hoang, S.D. Mahanti, Electronic structure of Ga-, In-, and Tl-doped PbTe: a supercell study

of the impurity bands, Phys. Rev. B. 78 (2008) 085111.

[22] C. Gayner, Y. Amouyal, Energy filtering of charge carriers: current trends, challenges, and prospects for thermoelectric materials. Adv. Funct. Mater. 30 (2020) 1901789.

[23] W.Y. Zhao, P. Wei, Q.J. Zhang, H. Peng, W.T. Zhu, D.G. Tang, J. Yu, H.Y. Zhou, Z.Y. Liu, X. Mu, D.Q. He, J.C. Li, C.L. Wang, X.F. Tang, J.H. Yang, Multi-localization transport behavior in bulk thermoelectric materials. Nat. Commun. 6 (2015) 6197.

[24] Y.Z. Pei, A.F. May, G.J. Snyder, Self-tuning the carrier concentration of PbTe/Ag_2Te composites with excess Ag for high thermoelectric performance. Adv. Energy Mater. 1 (2011) 291-296.

[25] H. Yang, J.H. Bahk, T. Day, A.M. Mohammed, G.J. Snyder, A. Shakouri, Y. Wu, Enhanced thermoelectric properties in bulk nanowire heterostructure-based nanocomposites through minority carrier blocking. Nano Lett. 15 (2015) 1349-1355.

[26] B. Paul, A. V. Kumar, P. Banerji, Embedded Ag-rich nanodots in PbTe: enhancement of thermoelectric properties through energy filtering of the carriers. J. Appl. Phys. 108 (2010) 064322.

[27] L.D. Zhao, J.Q. He, C.I. Wu, T.P. Hogan, X.Y. Zhou, C. Uher, V.P. Dravid, M.G. Kanatzidis, Thermoelectrics with earth abundant elements: high performance p-type PbS nanostructured with SrS and CaS. J. Am. Chem. Soc. 134 (2012) 7902-7912.

[28] K. Biswas, J.Q. He, I.D. Blum, C.I. Wu, T.P. Hogan, D.N. Seidman, V.P. Dravid, M.G. Kanatzidis, High-performance bulk thermoelectrics with all-scale hierarchical architectures, Nature 489 (2012) 414-418.

[29] Y. Pei, X. Shi, A. Lalonde, H. Wang, L. Chen, G.J. Snyder, Convergence of electronic bands for high performance bulk thermoelectrics, Nature 473 (2011) 66-69.

[30] D.L. Dexter, F. Seitz, Effects of dislocations on mobilities in semiconductors. Phys. Rev. 86 (1952) 964-965.

[31] Y.Z. Pei, Z.M. Gibbs, A. Gloskovskii, B. Balke, W.G. Zeier, G.J. Snyder, Optimum carrier concentration in n-type PbTe thermoelectrics, Adv. Energy Mater. 4 (2014) 1400486.

[32] H.T. Liu, Q. Sun, Y. Zhong, C.L. Xia, Y. Chen, Z.-G. Chen, R. Ang, Achieving high-performance n-type PbTe via synergistically optimizing effective mass and carrier concentration and suppressing lattice thermal conductivity. Chem. Eng. J. 428 (2022) 132601.

[33] B. Jabar, X.Y. Qin, D. Li, J. Zhang, A. Mansoor, H.X. Xin, C.J. Song, L.L. Huang, Achieving high thermoelectric performance through constructing coherent interfaces and building interface potential barriers in n-type $Bi_2Te_3/Bi_2Te_{2.7}Se_{0.3}$ nanocomposites. J. Mater. Chem. A. 7 (2019) 19120 - 19129.

[34] W.Y. Zhao, Z.Y. Liu, Z.G. Sun, Q.J. Zhang, P. Wei, X. Mu, H.Y. Zhou, C.C. Li, S.F. Ma, D.Q. He, P.X. Ji, W.T. Zhu, X.L. Nie, X.L. Su, X.F. Tang, B.G. Shen, X.L. Dong, J.H. Yang, Y. Liu, J. Shi, Superparamagnetic enhancement of thermoelectric performance. Nature 549 (2017) 247.

[35] M. Cutler, J.F. Leavy, R.L. Fitzpatrick, Electronic transport in semimetallic cerium sulfide. Phys. Rev. 133 (1964) A1143-A1152.

[36] J.Y.W. Seto, The electrical properties of polycrystalline silicon films. J. Appl. Phys. 46 (1975) 5247-5254.

[37] H. Wang, A.D. LaLonde, Y.Z. Pei, G.J. Snyder, The criteria for beneficial disorder in thermoelectric solid solutions. Adv. Funct. Mater. 23 (2013) 1586-1596.

[38] J.P. Heremans, C.M. Thrush, D.T. Morelli, Thermopower enhancement in PbTe with Pb precipitates, J. Appl. Phys. 98 (2005) 063703.

[39] Y.Z. Pei, N.A. Heinz, G.J. Snyder, Alloying to increase the band gap for improving thermoelectric properties of Ag_2Te. J. Mater. Chem. 21 (2011) 18256-18260.

[40] O. Madelung, Semiconductors: Data Handbook; Springer: Berlin, 2004.

[41] S.C. Erwin, L. Zu, M.I. Haftel, A.L. Efros, T.A. Kennedy, D.J. Norris, Doping semiconductor nanocrystals. Nature 436 (2005) 91-94.

[42] H.S. Kim, Z.M. Gibbs, Y.L. Tang, H. Wang, G.J. Snyder, Characterization of Lorenz number with Seebeck coefficient measurement, APL Mater. 3 (2015) 041506.

[43] D. Wu, L. D. Zhao, F. Zheng, L. Jin, M. G. Kanatzidis, J. Q. He, Understanding nanostructuring processes in thermoelectrics and their effects on lattice thermal conductivity. Adv. Mater. 28 (2016) 2737-2743.

[44] Y.Z. Pei, J. Lensch-Falk, E.S. Toberer, D.L. Medlin, G.J. Snyder, High thermoelectric performance in PbTe due to large nanoscale Ag_2Te precipitates and La doping, Adv. Funct. Mater. 21 (2011) 241-249.

[45] S.X. Liu, Y. Yu, D. Wu, X. Xu, L. Xie, X.L. Chao, M. Bosman, S.J. Pennycook, Z.P. Yang, J.Q. He, Coherent Sb/CuTe core/Shell nanostructure with large strain contrast boosting the thermoelectric performance of n-type PbTe, Adv. Funct. Mater. 31 (2020) 2007340.

[46] J. Zhang, D. Wu, D.S. He, D. Feng, M.J. Yin, X.Y. Qin, J.Q. He, Extraordinary thermoelectric performance realized in n-type PbTe through multiphase nanostructure engineering, Adv. Mater. 29 (2017) 1703148.

[47] C. Zhu, J. Zhang, H.W. Ming, X.N. Lou, L.L. Huang, T. Chen, B.L. Zhang, D. Li, H.X. Xin, X.Y. Qin, Enhanced thermoelectric performance of PbTe based materials by Bi doping and introducing MgO nanoparticles. Appl. Phys. Lett. 117 (2020), 042105.

[48] J. Callaway, H.C. von Baeyer, Effect of point imperfections on lattice thermal conductivity, Phys. Rev. 120 (1960) 1149-1154.

[49] T.J. Zhu, C.G. Fu, H.H. Xie, Y.T. Liu, B. Feng, J. Xie, X.B. Zhao, Lattice thermal conductivity and spectral phonon scattering in FeVSb-based half-Heusler compounds. EPL 104 (2013) 46003.

[50] A.D. LaLonde, Y.Z. Pei, G.J. Snyder, Reevaluation of $PbTe_{1-x}I_x$ as high performance n-type thermoelectric material, Energy Environ. Sci. 4 (2011) 2090-2096.

Table of Contents

Title: High-performance in n-type PbTe-based thermoelectric materials achieved by synergistically dynamic doping and energy filtering

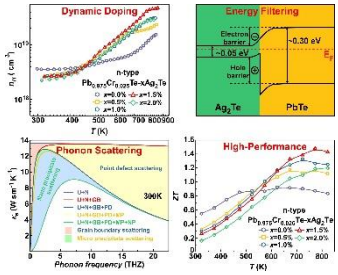

Ag_2Te nanoprecipitates introduce dynamic doping, energy filtering, and intense phonon scattering to simultaneously optimize the electrical and thermal properties of n-type Ag_2Te-alloyed $Pb_{0.975}Cr_{0.025}Te$, leading to a realization of high thermoelectric performance.

Author Information

Hang-Tian Liu is currently a Ph.D. candidate in Sichuan University under the supervision of Prof. Ran Ang. He received his B.S. from the School of National Defense Science and Technology College, Southwest University of Science and Technology, China, in 2017. His main research interests focus on the development of high-performance n-type PbTe thermoelectrics and the underlying physics.

Dr. Qiang Sun is currently a Beamline Scientist at the Centre of Microscopy and Microanalysis of the University of Queensland. He received his B.S. in Material Science & Engineering in 2013 from the University of Science and Technology Beijing and Ph.D. in Material Engineering in 2020 from the University of Queensland. His research interests include the synthesis, structure and applications of advanced functional materials for energy and biomedical applications.

Yan Zhong is currently a Ph.D. candidate in Sichuan University under the supervision of Prof. Ran Ang. She received her B.S. from the Environment and Safety Engineering College, University of South China, in 2018. Her current research focuses on the synthesis and properties of n-type PbTe thermoelectric materials.

Qian Deng is currently a Ph.D. candidate in Sichuan University under the supervision of Prof. Ran Ang. He received his B.S. from the School of Physics and Astronomy, Yunnan University, China, in 2020. His current research focuses on the synthesis and properties of PbSe thermoelectric materials.

Lin Gan is currently a Ph.D. candidate in Sichuan University under the supervision of Prof. Ran Ang. She received her B.S. and M.S. from the College of Nuclear Technology and Automation Engineering,

Chengdu University of Technology, China, in 2012 and 2015, respectively. Her current research focuses on the synthesis and properties of PbS thermoelectric materials.

Fang-Lin Lv is currently a M.S. candidate in Sichuan University under the supervision of Prof. Ran Ang. She received her B.S. from the College of Information Science and Engineering, Chengdu University, China, in 2020. Her current research focuses on the synthesis and properties of p-type PbTe thermoelectric materials.

Xiao-Lei Shi is currently a Research Fellow of Energy Materials at the University of Southern Queensland. He received his bachelor and master's degree in 2008 and 2011 from University of Science and Technology Beijing, respectively. He worked as a research and development engineer in Tsinghua University from 2012 to 2015, and received his Ph.D. degree in 2019 from the University of Queensland. His researches focus on the development of high-performance thermoelectrics and underlying physics and chemistry.

Zhi-Gang Chen is currently a Professor of Energy Materials in the University of Southern Queensland (USQ). He received his Ph.D. in materials science and engineering from the Institute of Metal Research, Chinese Academy of Science, in 2008. After his Ph.D., he had worked at the University of Queensland for seven years before moving to USQ, in 2016. His research concentrates on smart functional materials for thermoelectrics and nanoelectronics from synthesizing materials to understanding their underlying physics and chemistry.

Ran Ang is a Full Professor in Sichuan University since 2015. He received his PhD from the Institute of Solid State Physics, Chinese Academy of Sciences, in 2008, and his postdoctoral research experience spans 7 years during 2008–2015 from Nanyang Technological University; National University of Singapore; Tohoku University; and National Institute for Materials Science, Japan. He has been working on thermoelectric materials, superconducting materials, and magnetic materials for more than 18 years. His interests are focused on materials physics and thermoelectric applications.

Title:

High-performance in n-type PbTe-based thermoelectric materials achieved by synergistically dynamic doping and energy filtering

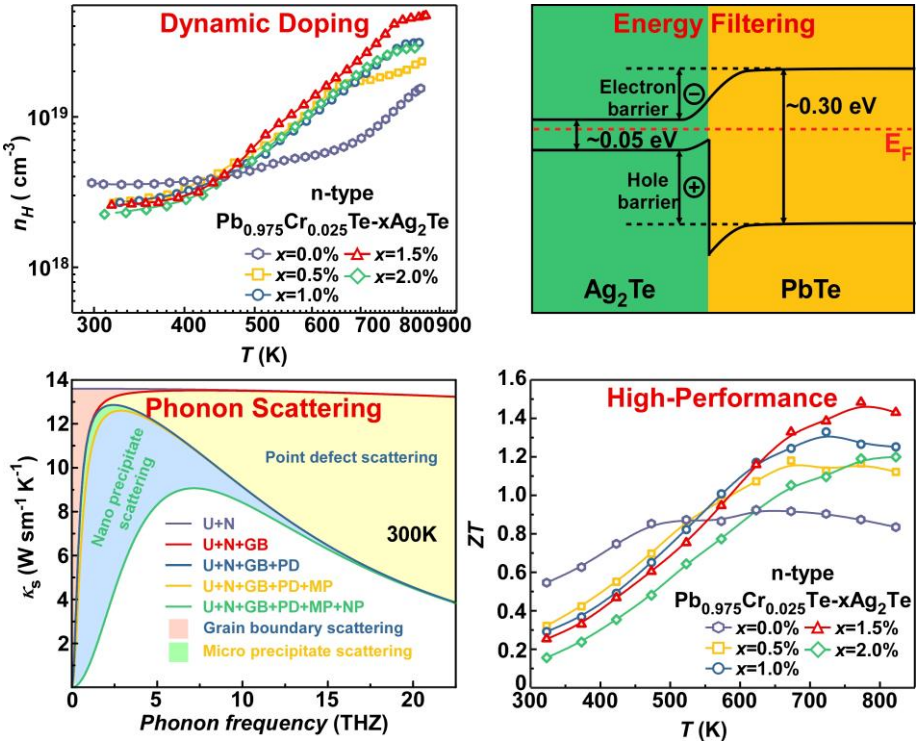

Graphical abstract

Ag_2Te nanoprecipitates introduce dynamic doping, energy filtering, and intense phonon scattering to simultaneously optimize the electrical and thermal properties of n-type Ag_2Te-alloyed $Pb_{0.975}Cr_{0.025}Te$, leading to a realization of high thermoelectric performance.

CRediT authorship statement

Hang-Tian Liu: Conceptualization, Methodology, Validation, Formal analysis, Investigation, Data curation, Visualization, Writing - original draft. **Qiang Sun:** Validation, Formal analysis, Investigation, Data curation, Visualization, Writing - original draft. **Yan Zhong:** Formal analysis. **Qian Deng:** Formal analysis. **Lin Gan:** Formal analysis. **Fang-Lin Lv:** Formal analysis. **Xiao-Lei Shi**: Validation, Writing - review & editing. **Zhi-Gang Chen:** Conceptualization, Validation, Formal analysis, Writing - review & editing, Supervision, Project administration. **Ran Ang:** Conceptualization, Methodology, Validation, Formal analysis, Writing - review & editing, Supervision, Project administration, Funding acquisition.